Improving modeling of ecosystem gross primary productivity through re-optimizing temperature restrictions on photosynthesis

Dong Yang [a,c], Xianli Xu [a,*], Fengjin Xiao [b], Chaohao Xu [a,c], Wei Luo [a,c], Lizhi Tao [d]

[a] *Huanjiang Observation and Research Station for Karst Ecosystem, Key Laboratory for Agro-ecological Processes in Subtropical Region, Institute of Subtropical Agriculture, Chinese Academy of Sciences, Changsha, Hunan 410125, China*
[b] *National Climate Center, Beijing 100081, China*
[c] *College of Resources and Environment, University of Chinese Academy of Sciences, Beijing 100049, China*
[d] *College of Resources and Environment Science, Hunan Normal University, Changsha, Hunan 410081, China*

HIGHLIGHTS

- The temperature restrictions on photosynthesis are re-optimized at ecosystem scale.
- A new ecosystem-scale temperature-based temperature stress factor is proposed.
- The performance of the novel model is better than MODIS GPP model.

GRAPHICAL ABSTRACT
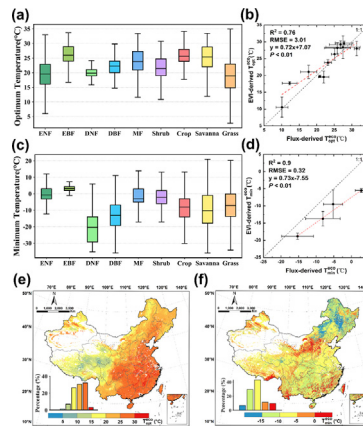
ARTICLE INFO

ABSTRACT

The terrestrial ecosystem gross primary productivity (GPP) plays an important role in the global carbon cycle and ecosystem functions. However, the estimates of GPP still have large uncertainties due to insufficient understanding of the photosynthesis-temperature relationship and maximum light use efficiency (LUE_{max}). We used satellite-derived proxies of GPP to derive optimum, minimum, and maximum temperature for photosynthesis at the ecosystem scale, which was then used to construct a new temperature stress expression. This study improves the MODIS-based light use efficiency model through coupling the optimized LUE_{max} with the new proposed temperature stress expression. The new model ($R^2 = 0.81$, RMSE = 17.8 gC m^{-2} (16 d)$^{-1}$) performed better than the MODIS GPP products ($R^2 = 0.67$, RMSE = 30.4 gC m^{-2} (16 d)$^{-1}$), especially for evergreen broadleaf forests and croplands. The mean annual GPP over China is 5.7 ± 0.27 PgC, and the GPP significantly increased by 0.046 ± 0.006 PgC year^{-1} during 2001–2018. This study provides a potential method for future projections of terrestrial ecosystem functioning.

* Corresponding author.
E-mail addresses: dongyang0318@gmail.com (D. Yang), xianlixu@isa.ac.cn (X. Xu), xiaofj@cma.gov.cn (F. Xiao), xuchaohao14@mails.ucas.edu.cn (C. Xu), 2009301610278@whu.edu.cn (W. Luo), lizhi_tao@163.com (L. Tao).

1. Introduction

Terrestrial ecosystem gross primary productivity (GPP) is widely known as the first step for terrestrial plants to absorb carbon from the

atmosphere through photosynthesis. It describes the assimilation effect of vegetation on photosynthetic carbon (Monteith, 1972) and also represents the largest carbon dioxide (CO_2) flux between the terrestrial biosphere and atmosphere (Beer et al., 2010). The change in GPP would significantly alter global carbon cycling and ecosystem functions, and thus feedback to the climate (Fernández-Martínez et al., 2014; Piao et al., 2009; Yao et al., 2018). As a result, understanding GPP and its spatiotemporal variation will reveal the response of ecosystems to climate change and improve our understanding of the terrestrial carbon cycle.

To date, various models have been developed to estimate GPP, among which remote sensing data-driven models have provided an unprecedented opportunity for better regional/global GPP estimations (Li and Xiao, 2019). Remote sensing data-driven models are commonly based on the light-use-efficiency (LUE) theory, which states that GPP can be formulated as the product of the LUE and the absorbed photosynthetically active radiation (APAR) (Monteith, 1972).

$$GPP = LUE \times APAR = LUE_{max} \times f_{stress} \times FPAR \times PAR \qquad (1)$$

where LUE_{max} is the maximum LUE, which is either a constant (Potter et al., 1993) or changes in different ecosystems (Running et al., 2000); f_{stress} refers to the maximum LUE reduction under environmental stresses; PAR is the incident photosynthetically active radiation; $FPAR$ is the fraction of incident PAR absorbed by the surface, usually derived from remote sensing data. Although these models have unclear ecological mechanisms, they have been widely globally due to simplicity of their theory and the availability of relatively long-term and large-scale remote sensing data (Ogutu et al., 2013). The Moderate Resolution Imaging Spectroradiometer (MODIS) GPP model (MOD17) is the most widely used GPP model based on the LUE theory (Running et al., 2004). It offers a global-scale GPP product at high spatial (500 m) and temporal (8-days) resolutions, useful for monitoring and simulating the global carbon cycle (Running et al., 2004). However, large uncertainties still exist in the MOD17 algorithm arising from the parameterization of the biome-specific lookup table, the inputs of data, and the algorithm itself (Heinsch et al., 2006; Turner et al., 2006; Wang et al., 2017; Yuan et al., 2014).

Similar to many GPP estimation models, temperature is considered a primary environmental stress affecting LUE_{max} in MOD17 algorithm. These models usually use a biome-specific look-up table, in which fixed air temperature parameters are defined for each vegetation type (Running et al., 2004; Xiao et al., 2004a; Yan et al., 2015; Yuan et al., 2007). However, the temperature effect on ecosystem photosynthesis is spatially heterogeneous (Liu et al., 2017) because of scaling differences among single species, plant communities, or ecosystems. Several studies reported that the biome-specific parameters for each vegetation type do not vary with time or space might lead to high uncertainties in quantifying GPP (White et al., 2000). Moreover, MOD17 only considers the minimum temperature to limit plant growth and ignores the effect of high temperature on ecosystem photosynthesis. When the minimum temperature of different vegetation types exceeds 8–12 °C, the MOD17 algorithm considers that the vegetation is no longer subject to temperature restrictions. However, appropriate temperature increases the activity of enzymes and accelerates plant growth (Kattge and Knorr, 2007), while inappropriate temperatures tend to inhibit the carbon fixation process of vegetation photosynthesis (Smith et al., 2016). High temperatures are thought to influence plant physiological processes (e.g., reducing stomatal conductance, enzyme activity, and promoting photosynthetic carbon metabolism) and vegetation canopy (e.g., leaf withering and senecence) (Bjorkman and Demmig, 1987; Hunt et al., 2004; Zhang et al., 2016), thereby severely affecting vegetation photosynthesis. In addition, these models generally simplify the mechanism of temperature requirements for vegetation growth and use the knowledge from leaf-scale or provide simplified definitions of the photosynthesis-temperature relationship (Liu, 2020). A recent research by Huang et al. (2019) showed that the ecosystem-scale optimum

temperature (T_{opt}^{eco}) is consistently lower than the leaf-scale optimum temperature (T_{opt}^{leaf}) and reported the first global distribution of the T_{opt}^{eco}. However, they did not study and discuss other ecosystem-scale photosynthesis-temperature further (minimum and maximum temperature). An understanding of the temperature lower and upper limits helps to promote the estimation of GPP. In addition to using a limited number of eddy covariance flux towers, it is also possible to use vegetation indices (e.g., EVI) as satellite proxies for photosynthesis to quantify the related photosynthesis-temperature parameters at the ecosystem scale (Chang et al., 2021; Chang et al., 2020).

The MOD17 algorithm assumes that the LUE_{max} remains constant for each vegetation type, and the APAR is the energy absorbed by the entire canopy (Running et al., 2004). However, some researchers have suggested that the photosynthetic capacity is mainly affected by leaf chlorophyll content in the canopy (Houborg et al., 2013; Wu et al., 2016). Compared with FPAR derived from the whole canopy, the fraction of PAR absorbed by chlorophyll ($FPAR_{chl}$) can better capture the seasonal variation of vegetation photosynthetic capacity (Ogutu and Dash, 2013; Zhang et al., 2009; Zhang et al., 2014; Zhou et al., 2017). Considering the superiority of $FPAR_{chl}$ in GPP estimation, many GPP estimation models based on $FPAR_{chl}$ have been developed (Gao et al., 2014; Gitelson et al., 2006; Sims et al., 2008; Xiao et al., 2004a). Moreover, some studies have suggested that LUE_{max} is underestimated in many areas (Kattge et al., 2009; Liu et al., 2014). These problems led to relatively low temporal and spatial representations of MOD17 at site-level validation and large-scale underestimation, especially for evergreen broadleaf forests and croplands (Turner et al., 2006; Wang et al., 2017; Zhang et al., 2012). Therefore, improving the MODIS GPP algorithm for these shortcomings is of great importance to the study of the terrestrial carbon cycle.

As a large country with almost all ecosystem types and with the terrestrial ecosystems having great carbon sequestration potential in the global carbon budget (Piao et al., 2009; Wang et al., 2020), China is an ideal study region. Here, we examine the potential of using satellite-derived proxies of GPP (Enhanced Vegetation Index [EVI]) to estimate spatially explicit ecosystem-scale temperature parameters of vegetation productivity. To achieve this, a new temperature stress factor was established in this study, which was compared with the temperature stress factor in MODIS GPP products. Furthermore, we developed a novel MODIS-based light use efficiency model coupled with the optimized LUE_{max} and new temperature stress factor. The ability of GPP simulation was examined and compared with the MODIS GPP products, and the GPP of China was further estimated.

2. Materials and methods

2.1. Materials

2.1.1. Eddy covariance flux data

A total of 11 typical flux-tower sites with 70 site years of flux data across China were used in this study (Fig. 1). Detailed information can be found in Table 1. Quality-controlled half-hourly observations (including GPP and climate data) were obtained from ChinaFLUX (www.chinaflux.org) and global FLUXNET data network (www.fluxnet.org) (Papale et al., 2006; Pastorello et al., 2020; Yu et al., 2013). All the half-hourly observed flux data were transformed into a daily and 16-day resolution for further analysis. All flux-tower verified measurements were divided into two groups for model calibration and validation.

2.1.2. Meteorological data

Meteorological data (including daily mean temperature and relative humidity and daily sunshine hour data) at approximately 2474 weather stations were collected by the China Meteorological Administration (CMA) (http://data.cma.cn/) from 2000 to 2018. Radiation data were
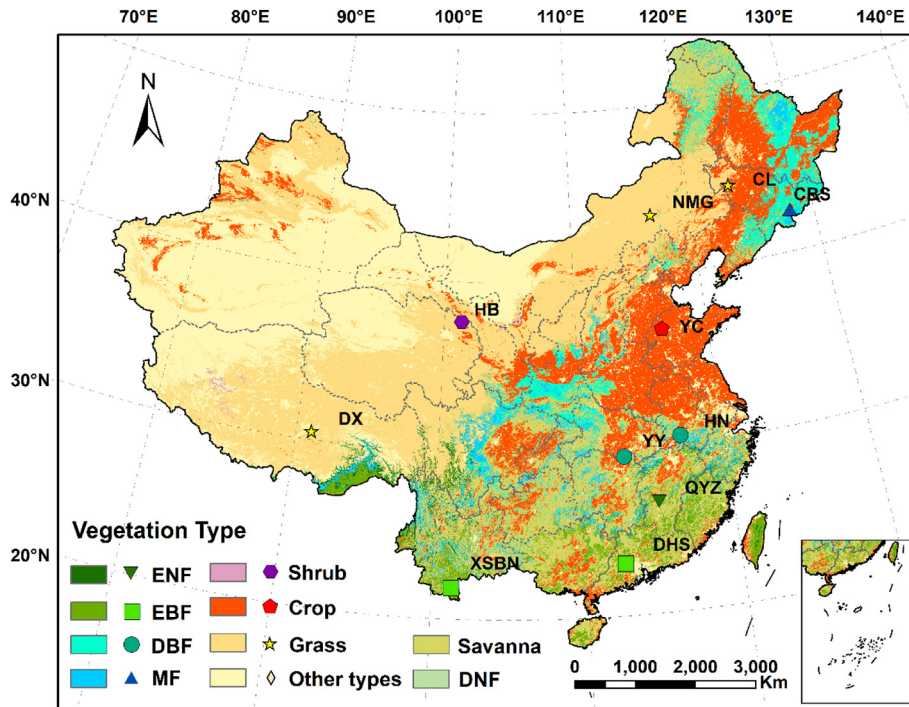
Fig. 1. Distribution of flux-tower sites in China used in this study. Different symbols in the figure indicate flux-tower sites of different vegetation types with a similar color to the same vegetation type. EBF: Evergreen Broadleaf Forest; ENF: Evergreen Needleleaf Forest; DNF: Deciduous Needleleaf Forest; DBF: Deciduous Broadleaf Forest; MF: Mixed forests; Crop: Croplands; Grass: Grasslands; Shrub: Closed Shrublands and Open Shrublands; Savanna: Woody Savannas and Savannas; Other types: Water, Snow, Urban, and Barren.

also obtained from the CMA, based on sunshine hour, air temperature, humidity, and other data and derived from the comprehensive solar radiation estimation model. Based on the MODIS GPP algorithm, PAR is calculated to be 45% of the total shortwave radiation (Running et al., 2004). The vapor pressure deficit (VPD) was derived using the World Meteorological Organization Commission for Instruments and Methods of Observation Guide conversion equation based on air temperature and relative humidity data (Chiang et al., 2018). The meteorology data were calculated within the same 16-day periods to be consistent with the time scale of the MODIS data.

Then, we used thin plate-smoothing spline-fitting techniques in ANUSPLIN 4.4 (Hutchinson and Xu, 2013) to interpolate the meteorological data into a 1 km spatial resolution over entire China with latitude, longitude and elevation as covariates. Elevation data were obtained from the Shuttle Radar Topographic Mission product (Jarvis A et al., 2008). All observed meteorological data series were quality

controlled and observed flux-tower climate data were applied as independent observations to evaluate the interpolated products. The results showed that the meteorological interpolation data interpolated were useful, and its accuracy was high (Fig. S1).

2.1.3. MODIS data

MODIS products (MOD13Q1, MOD17A2H, MOD15A2H, and MCD12Q1) in the period to 2001–2018 were archived at the National Aeronautics and Space Administration (NASA) Distributed Active Archive Center (DAAC). EVI is a vegetation index that has minimized canopy–soil variations and improved sensitivity over high biomass regions (Didan, 2015). We used a 16-day EVI dataset with a spatial resolution of 250 m from the MOD13Q1 vegetation index product. FPAR is the fraction of photosynthetically active radiation absorbed by vegetation and is acquired from the 500 m spatial resolution, 8-day products (MOD15A2H) (Myneni et al., 2015). All low quality data of EVI/FPAR data were checked,

Table 1
Site characteristics in this study.

Site ID	Site name	Latitude (°N)	Longitude (°E)	Data range	Vegetation type	Climate	T_{opt}^{eco} (°C)[a]	T_{min}^{eco} (°C)[b]
QYZ	Qianyanzhou	115.05	26.73	2003–2010	ENF	Subtropical	26.8	–
DHS	Dinghushan	112.5	23.15	2003–2010	EBF	Subtropical	27.8	–
XSBN	Xishuangbanna	101.267	21.9	2003–2010	EBF	Tropical	25.1	–
YY[c]	Yueyang (CN-Hny)	112.93	29.53	2005–2006	DBF	Subtropical	31.4	–
HN[c]	Huaining (CN-Anh)	116.98	30.48	2005–2006	DBF	Subtropical	27.5	–
CBS	Changbaishan	128.0958	42.4025	2003–2010	MF	Temperate	22	−5.2
HB	Haibei	101.33	37.6652	2003–2010	Shrub	Alpine	12.3	−8.1
DX	Dangxiong	91.066	30.497	2004–2010	Grass	Alpine	10.1	2.8
NMG	Neimenggu	116.667	43.53	2004–2010	Grass	Temperate	17.7	–
CL[c]	Changling (CN-Cng)	123.5092	44.5934	2007–2010	Grass	Temperate	23.2	−13.7
YC	Yucheng	116.567	36.83	2003–2010	Crop	Temperate	25.9	–

[a] T_{opt}^{eco}: The ecosystem-scale optimal temperature for vegetation productivity.
[b] T_{min}^{eco}: The ecosystem-scale minimum temperature for vegetation productivity.
[c] Data from sites were obtained from www.fluxnet.org, other were www.chinaflux.org.

and data gaps were filled using linear temporal interpolation (Zhao et al., 2005). The Savitsky–Golay smoothing filter was used to remove the noise of EVI and FPAR data induced by cloudy, snow and atmospheric contamination (Jonsson and Eklundh, 2004). MOD17A2H GPP products (MOD17) (Running and Zhao, 2019) were used to evaluate the improved GPP model. Furthermore, 8-day FPAR and GPP data were transformed to 16-day for conforming to EVI data in this study. For each flux-tower site, MOD17, EVI, and FPAR were extracted from 3×3 km around the center pixel of the flux-tower sites (Liu et al., 2014).

We used MODIS land cover with the classification scheme of the International Geosphere-Biosphere Program (IGBP). The MODIS IGBP land cover data were derived from the MCD12Q1 Land Cover Science Data Product at a spatial resolution of 1 km (Friedl and Sulla-Menashe, 2019). The 17 land cover types were reclassified into nine vegetation types: evergreen broadleaf forest (EBF), evergreen needle-leaf forest (ENF), deciduous needle-leaf forest (DNF), deciduous broadleaf forest (DBF), mixed forests (MF), woody savannas, savannas (Savanna), croplands (Crop), grasslands (Grass), and closed shrublands and open shrublands (Shrub). Land cover types of water, snow, urban, and barren are treated as non-vegetated areas (other types). The spatial distribution of the nine vegetation types is also shown in Fig. 1 with a lighter color than flux-tower sites in the same class.

2.2. Methods

2.2.1. Determinations of the temperature parameters for photosynthesis

Similar to previous research (Huang et al., 2019; Niu et al., 2012; Zhou et al., 2015), we used productivity observations (flux GPP data) and proxies (satellite-derived EVI) to calculate and map the ecosystem-scale optimal air temperature (T_{opt}^{eco}) for vegetation productivity. Furthermore, we estimated the local ecosystem-scale minimum (T_{min}^{eco}) and maximum air temperature (T_{max}^{eco}) of vegetation productivity by examining the temperature response curve of GPP and EVI.

First, EVI and weather-station-data-derived temperature time series from 2000 to 2018 were grouped into different 1 °C temperature bins for each vegetated pixel. The influence of other environmental constraints was reduced by using the 90% quantile of the EVI data as the EVI response in each temperature bin and calculating the moving average of every three temperature bins. The temperature response curve of photosynthesis is generally bell-shaped and the T_{opt}^{eco} was determined from the temperature response curve at which EVI was maximized (Fig. 2). The T_{min}^{eco} and T_{max}^{eco} were determined from the temperature response curve at which EVI was less than 0.1 (Fig. 2). Sims et al. (2006) pointed out GPP is almost 0 when EVI is approximately 0.1 (Sims et al., 2006), which was proved by our results (Fig. S2). Note that the T_{opt}^{eco} cannot be attained at either end of the response curve. Moreover, the T_{min}^{eco} must be less than the T_{opt}^{eco}, and the T_{max}^{eco} must be greater than the T_{opt}^{eco}. These pixels that cannot detect T_{opt}^{eco}, T_{min}^{eco}, and T_{max}^{eco} and unvegetated pixels (multi-annual EVI values less than 0.1) (Seddon et al., 2016) were set to be NODATA. NODATA was replaced with the average values of T_{opt}^{eco} and T_{min}^{eco} in the same ecotype region, respectively. Regarding T_{max}^{eco}, it is difficult to detect. Its values refer to the settings of the Terrestrial Ecosystem Model (Aber et al., 1996; McGuire et al., 1992) on different vegetation types, as shown in Table 2. The reasons for this are discussed in Section 4.

The same method used for the EVI-derived T_{opt}^{eco} and T_{min}^{eco} was used to estimate the Flux-derived T_{opt}^{eco} and T_{min}^{eco} for each site year with time series of daily GPP data and corresponding temperature data derived from flux-tower observations. The T_{opt}^{eco} was determined from the temperature response curve at which GPP was maximized and the T_{min}^{eco} were determined from the temperature response curve at which GPP was almost 0. The EVI-derived T_{opt}^{eco} and T_{min}^{eco} were compared with Flux-derived T_{opt}^{eco} and T_{min}^{eco} using a least-square linear regression at all 11 flux-tower sites. We calculated the mean and standard deviation of
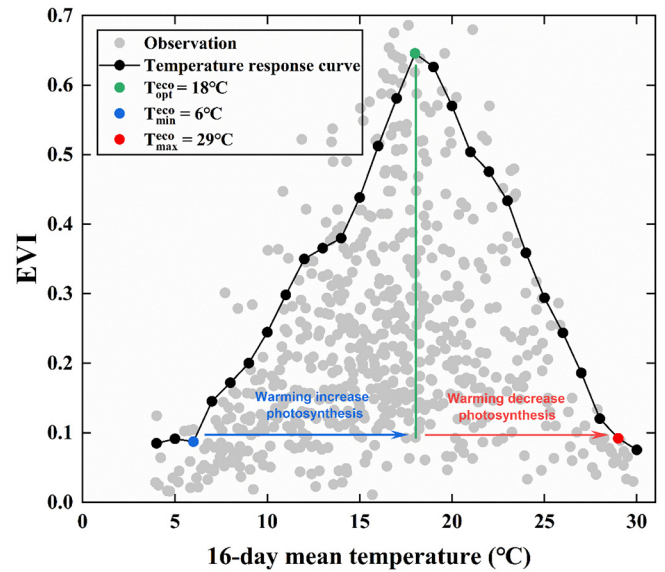
Fig. 2. The definition of ecosystem-scale optimum, minimum and maximum temperature for photosynthesis (T_{opt}^{eco}, T_{min}^{eco} and T_{max}^{eco}) with an example of a pixel. Gray dots indicate the observed MODIS EVI and the corresponding 16-day-averaged air temperature from 2001 to 2018, and black dots are the 90% quantile for each 1 °C temperature bin.

each temperature parameter based on each site year with daily GPP and corresponding temperature data for each flux-tower site. We then extracted and calculated the mean and standard deviation of each temperature parameter within 3×3 pixels around each flux-tower site center from the EVI-derived T_{opt}^{eco} and T_{min}^{eco} map.

2.2.2. Model descriptions

The MODIS GPP algorithm is based on the Monteith LUE theory (1972),

$$GPP = LUE_{max} \times f(TMIN) \times f(VPD) \times FPAR \times PAR \qquad (2)$$

where LUE_{max} is the maximum conversion efficiency in different vegetation types, PAR is the incident photosynthetically active radiation, and $FPAR$ is the fraction of PAR absorbed by the canopy. $f(VPD)$ and $f(TMIN)$ represent the limitations of vapor pressure deficit and minimum air temperature on GPP and can be calculated as follows:

$$f(VPD) = \frac{(VPD_{max} - VPD)}{(VPD_{max} - VPD_{min})} \qquad (3)$$

$$f(TMIN) = \frac{(TMIN - TMIN_{min})}{(TMIN_{max} - TMIN_{min})} \qquad (4)$$

where VPD is the vapor pressure deficit (Pa), $TMIN$ is the minimum air temperature (°C), and VPD_{max}, VPD_{min}, $TMIN_{max}$, and $TMIN_{min}$ are parameters dependent on vegetation types. $f(VPD)$ and $f(TMIN)$ are simple linear ramp functions of $TMIN$ and VPD, respectively, with both ranging from 0 to 1, as illustrated in Fig. S2a and b. A more detailed description of the MODIS GPP model can be found in the literature (Running et al., 2004).

This study developed an improved model to estimate GPP based on the MODIS GPP model algorithm. One improvement is to improve the limitation that the $f(TMIN)$ expression ignores the influence of high temperature and spatial heterogeneity. We integrate the ecosystem-scale temperature parameters into a new temperature stress expression and define $f(T)$ with the following equation, showing that photosynthesis is suppressed at lower and higher air temperature thresholds. The $f(T)$ also ranges from 0 to 1, as illustrated in Fig. S2c.

Table 2

Parameters of ecosystem-scale maximum temperature for photosynthesis (T_{max}^{eco}) and calibrated maximum light use efficiency (LUE_{max}) for different vegetation types.

Vegetation type	EBF	ENF	DNF	DBF	MF	Shrub	Savanna	Crop	Grass
LUE_{max} (gC/m^2)	2.4634	2.8348	2.1962	1.5005	2.4829	1.6422	2.1962	3.2551	1.1948
T_{max}^{eco} (°C)	48	40	40	40	48	48	48	48	48

$$f(T) = min\left(\frac{T_a - T_{min}^{eco}}{T_{opt}^{eco} - T_{min}^{eco}}, \frac{T_{max}^{eco} - T_a}{T_{max}^{eco} - T_{opt}^{eco}}\right) \qquad (5)$$

where T_a is the air temperature (°C), and T_{opt}^{eco}, T_{max}^{eco}, and T_{min}^{eco} are the ecosystem-scale optimum, maximum and minimum temperatures for photosynthesis activities, respectively. T_{opt}^{eco}, T_{min}^{eco}, and T_{max}^{eco} are estimated by the method in Section 2.2.1. The value of T_{max}^{eco} is based on the vegetation type and can be found in Table 2.

The $f(TMIN)$ indicated temperature stress was used in the MODIS GPP model while the $f(T)$ applied in this study. We evaluated their potential in representing the temperature stress effect in two ways. First, the Pearson's correlation analysis was applied to explore the relationship between the 16-day observed GPP vs. $f(T)$ and $f(TMIN)$ at the 11 flux-tower sites. Because there is no minimum air temperature observation data at most flux-tower sites, we calculated $f(TMIN)$ using the minimum temperature data extracted from interpolated meteorological data around each site center. Second, we calculated a new GPP (MOD_T) for flux-tower sites on a 16-day scale with $f(T)$ to substitute for $f(TMIN)$ in the original MODIS GPP algorithm.

Another improvement is to replace FPAR with FPAR$_{chl}$ and optimize the corresponding LUE$_{max}$. FPAR$_{chl}$ is often represented by EVI according to previous studies (Wu et al., 2010; Xiao et al., 2004b). Pearson's correlation analysis was also conducted for the 16-day observed GPP vs. FPAR (EVI) at 11 flux-tower sites. The corresponding LUE$_{max}$ of the improved model was calibrated based on flux-tower GPP data by using the evolutionary algorithm in this study. The evolutionary algorithms are robust and powerful tools for solving the global optimization problem and the GEATbx (Genetic and Evolutionary Algorithm Toolbox) in MATLAB was implemented in our analysis (Pohlheim, 2006). Then, we calculated a new GPP (MOD_F) for flux-tower sites on a 16-day scale with $f(T)$, EVI, and optimized LUE$_{max}$ to substitute for the corresponding expression and parameters in the original MODIS GPP algorithm.

2.2.3. Model validation and comparisons

To distinguish the impacts of meteorological data on GPP, we calculated a new GPP (MODIS_Me) for flux-tower sites on a 16-day scale. MODIS_Me was based on the MODIS GPP algorithm and was driven by meteorology data extracted from interpolated meteorological data around each site center. Finally, the performance of the MOD_Me, MOD_T, MOD_F, and MODIS GPP product (MOD17) were evaluated by comparing GPP values measured by flux-tower sites. The statistical indices used for evaluation were the coefficient of determination (R^2), and root-mean-square-error (RMSE). It is commonly accepted that the smaller the RMSE and the closer the R^2 value is to 1, the better the model performance (Moriasi et al., 2007; Xu et al., 2020).

2.2.4. Trend analysis of GPP

We quantified the long-term trend in annual GPP for each grid cell between 2001 and 2018 using the non-parametric Mann-Kendall (MK) test (Kendall, 1975; Mann, 1945). This method is frequently used for the significance of trend analysis of vegetation variables (Xie et al., 2019). The trends with $P \leq 0.05$ were considered statistically significant in this study.

3. Results

3.1. Temperature parameters for photosynthesis

Flux-derived T_{opt}^{eco} and T_{min}^{eco} values ranged from 10.1–31.4 °C and −5.8–2.1 °C, respectively (Table 1). Generally, T_{min}^{eco} cannot be detected in tropical and subtropical sites (XSBN, DHS, QYZ, YY, and HN) and T_{opt}^{eco} in tropical and subtropical sites is higher than that in temperate and alpine sites (Table 1), implying a dependency of T_{opt}^{eco} and T_{min}^{eco} on the background climate. The satellite observations of EVI are also used to estimate and map the spatial distribution of T_{opt}^{eco} and T_{min}^{eco} in China (Fig. 3e and f). EVI-derived T_{opt}^{eco} and T_{min}^{eco} are comparable to those from measurements of flux-tower sites (Fig. 3b and d), which support using the EVI proxy to map T_{opt}^{eco} and T_{min}^{eco}.

The average EVI-derived T_{opt}^{eco} and T_{min}^{eco} over the vegetated areas of China was 22.5 ± 5 °C and −7.7 ± 5.3 °C with a high spatial heterogeneity, respectively. Fig. 3e shows that T_{opt}^{eco} in most areas varies within the range of 15–30 °C, and T_{opt}^{eco} in the eastern region is generally larger than that in the western region (Fig. 3e). Maximum values of T_{opt}^{eco} near 30 °C prevail at southeastern China and subtropical regions, while minimum values close to 10 °C mainly appear in high altitudes and Tibetan Plateau regions. As shown in Fig. 3f, over 70% of the T_{min}^{eco} varies within −15 to −5°. Maximum values of T_{min}^{eco} close to 0 °C mainly appear in evergreen broad-leaved forests, while minimum values near −15 °C prevail at high latitudes and cold regions. Vegetation-specific T_{opt}^{eco} and T_{min}^{eco} were investigated for the nine vegetation types in China (Fig. 3a and c). Among the nine vegetation types, the largest mean T_{opt}^{eco} was found in the evergreen broad-leaved forest (26 ± 4.7 °C), while the smallest mean T_{opt}^{eco} (18.9 ± 5.1 °C) was found in grasslands (Fig. 3a). Evergreen broad-leaved forest also has the largest T_{min}^{eco}, with a value of 3.3 ± 2.9 °C, while deciduous broad-leaved forest has the smallest T_{min}^{eco} with a value of −20.4 ± 9.1 °C (Fig. 3c).

3.2. Parameters of the improved model

Correlation analysis showed that observed GPP had a better correlation with $f(T)$ than that with $f(TMIN)$ at most sites (Fig. 4a), especially in all forest flux-tower sites. There was almost no correlation between the observed GPP and $f(TMIN)$ in the two EBF sites (XSBN and DHS); however, the correlation coefficients of observed GPP and $f(T)$ at XSBN and DHS flux-tower sites were 0.87 and 0.68, respectively. The correlations between observed GPP and EVI are also better than those between GPP and FPAR in forest flux-tower sites (Fig. 4b). The lowest correlations between observed GPP and FPAR were in the two EBF sites (XSBN and DHS) at 0.22 and 0.49, while the correlations between observed GPP and EVI are as high as 0.57 and 0.68, respectively.

Table 2 shows the optimized LUE$_{max}$ for the improved GPP model (MOD_F). The optimized LUE$_{max}$ of all vegetation types was higher than that of the original MOD17 and exhibited extensive variability across vegetation types. The optimized LUE$_{max}$ of cropland was higher than those of the other flux-tower sites, while grassland was the lowest among all vegetation types. Due to the lack of DNF and Savanna flux-tower sites, the average LUE$_{max}$ from all other tower sites was used for these two vegetation types.
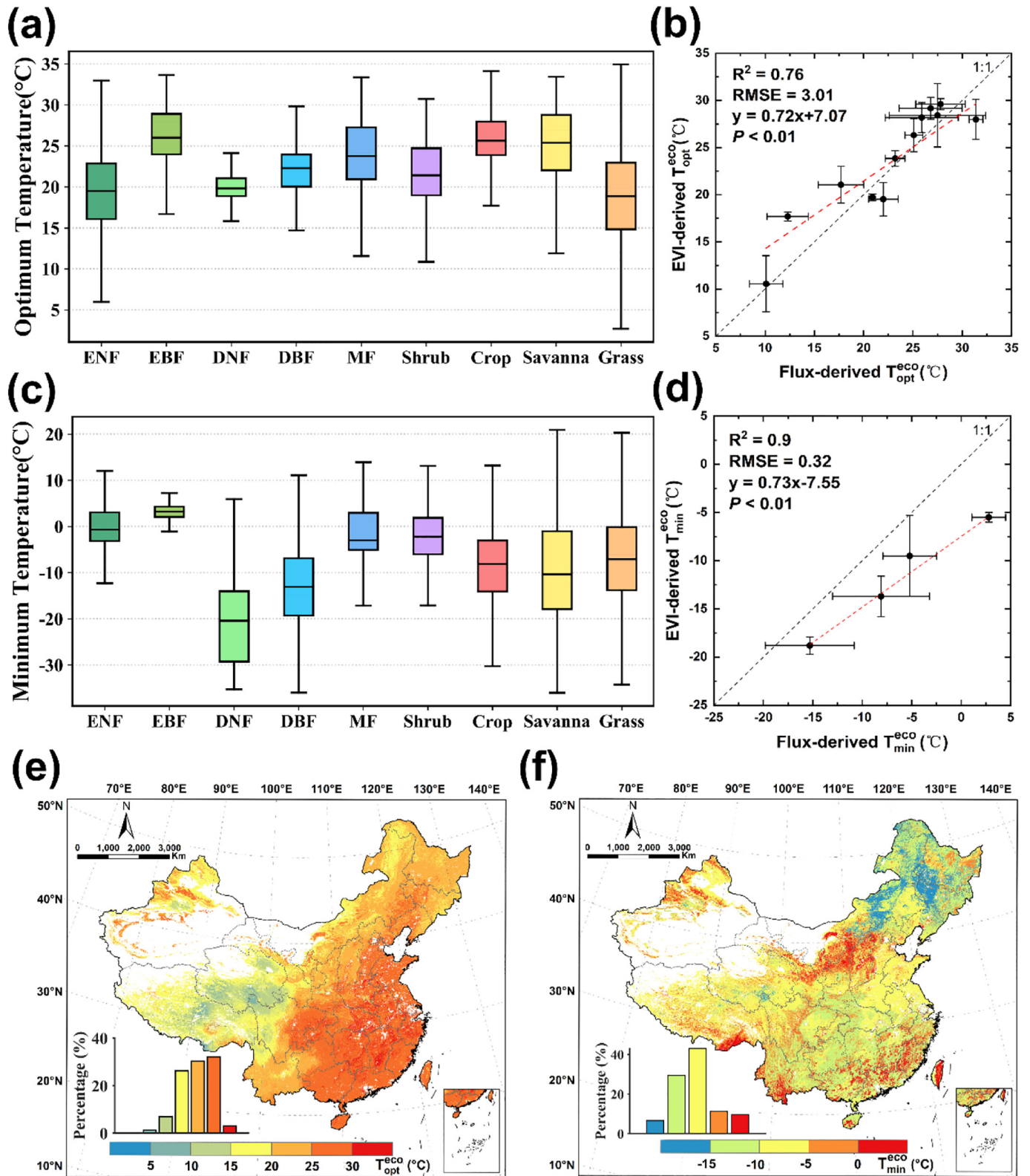
Fig. 3. (a, c) Box plot of ecosystem-scale optimum and minimum temperature for photosynthesis (T_{opt}^{eco} and T_{min}^{eco}) for different vegetation types across China; (b, d) relationships between flux and EVI-derived T_{opt}^{eco} and T_{min}^{eco}; (e, f) spatial distribution of T_{opt}^{eco} and T_{min}^{eco}. Horizontal lines in the box indicate the average T_{opt}^{eco} and T_{min}^{eco}, and the shaded area with different colors refers to the distribution of T_{opt}^{eco} and T_{min}^{eco} values (a, c); Black spot and error bars indicate means $\pm$ standard deviation (b, d); The inset in panel (e, f) denotes the frequency distribution of T_{opt}^{eco} and T_{min}^{eco}.

3.3. Performance of the improved model

The improving GPP estimates (MOD_T and MOD_F) were compared with the original MOD17, MOD_Me, and observed GPP data in the validation period (Fig. 5). MOD_F had the highest R^2 and lowest RMSE at the site level of all models. The R^2 value of MOD_F against observed GPP ranged from 0.56 (XSBN) to 0.98 (HB), and RMSE ranges from 5.04 gC m^{-2} (16 d)$^{-1}$ (DX) to 49.24 gC m^{-2} (16 d)$^{-1}$ (YC). The
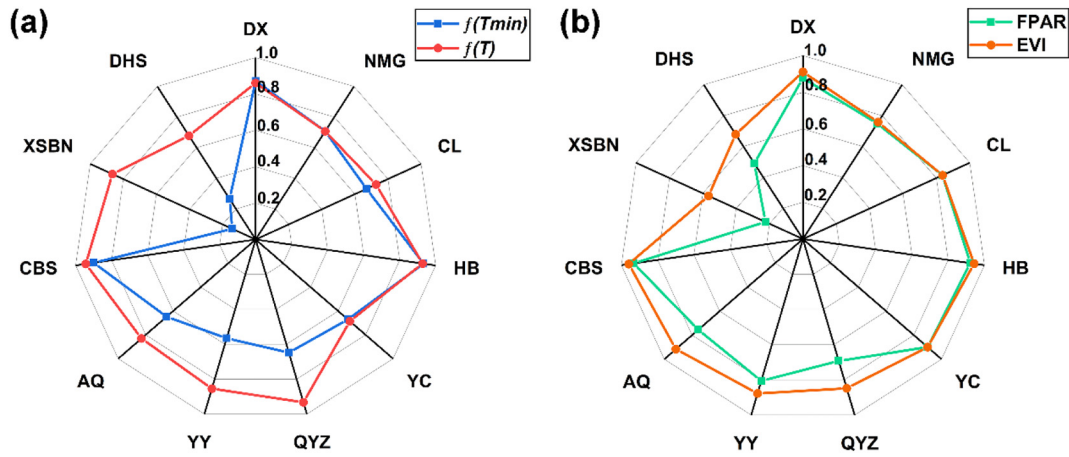
Fig. 4. Correlation coefficients of observed GPP vs. $f(T)$ and $f(TMIN)$ (a), and observed GPP vs. FPAR and EVI (b) at 11 flux-tower sites, respectively. DHS, DX, NMG, CL, DL, HB, YC, QYZ, YY, HN, CBS, and XSBN are the flux-tower site ID. Detailed information can be found in Table 1.

performance of MOD_T (site-mean R^2, and RMSE are 0.74, and 26.86 gC m^{-2} (16 d)$^{-1}$, respectively) is also better than that of MOD17. Overall, it can be seen that $f(T)$, as a temperature stress factor in the improved GPP model, had a better capacity to represent the temperature stress effect. The performance of the XSBN site is worse than that of other sites, especially in MOD17 and MOD_Me. Although there are some improvements in MOD_T, the R^2 value at the XSBN site is still small. However, the performance of the XSBN site in MOD_F was greatly improved, and R^2 was 0.56, and RMSE was 23.36 gC m^{-2} (16 d)$^{-1}$.

The MOD_Me and MOD17 had almost identical performance (site-mean R^2 was 0.67, and RMSE was 29.4, and 30.4 gC m^{-2} (16 d)$^{-1}$, respectively). This performance suggests that the different input meteorological data sources do not significantly impact the GPP simulation results. MOD17 and MOD_Me are both lower than observed GPP at all flux-tower sites, except for the DHS sites (Fig. 6). They show an apparent underestimation, especially in the grass (DX, CL) and crop (YC) sites, which is consistent with previous studies (Yan et al., 2015; Zhang et al., 2008). Such findings may be due to the lower default LUE$_{max}$ values used to produce the MODIS GPP product. The MOD_F is consistent with the observed GPP in the validation years at each site. Therefore, the improved MOD_F is the best when considering performance and seasonal variations among all models.

3.4. Spatiotemporal patterns of GPP over China

The spatial pattern of the mean annual GPP estimated by the MOD_F model is shown in Fig. 7a. The magnitude of the mean annual GPP in more than 40% of the regions ranged from 1000 to 2000 gC m^{-2}. The highest mean annual GPP is distributed in northern China and tropical regions such as Hainan and the southern Yunnan Province, the intermediate values in the regions of central and southeast China, and the lowest values in northwest China, Qinghai-Tibet, and barren regions. Compared with MOD17, the MOD_F model produces similar spatial patterns of mean annual GPP (Fig. 7b); however, MOD17 shows lower GPP estimates than MOD_F in the northeast and north China and Qinghai-Tibet regions. These regions are mostly dominated by deciduous broadleaf forest, cropland, and grassland (Fig. 1).

The temporal trends of annual GPP estimated by MOD_F and MOD17 are shown in Fig. 7c and d, respectively. During the period of 2001 to 2018, almost 39.2% of the vegetated area in China showed a statistically significant trend in GPP ($P < 0.05$). The areas with a positive trend (90%) are more widespread than those with negative trends (Fig. 7c). Only a few decreases in GPP occurred in some eastern and northernmost parts of China. MOD17 shows similar spatial patterns of annual GPP temporal, and positive trends are also more widespread (97%, Fig. 7d). The magnitude of the trend in most areas varies from 0 to 20 gC m^{-2} year^{-1}, and
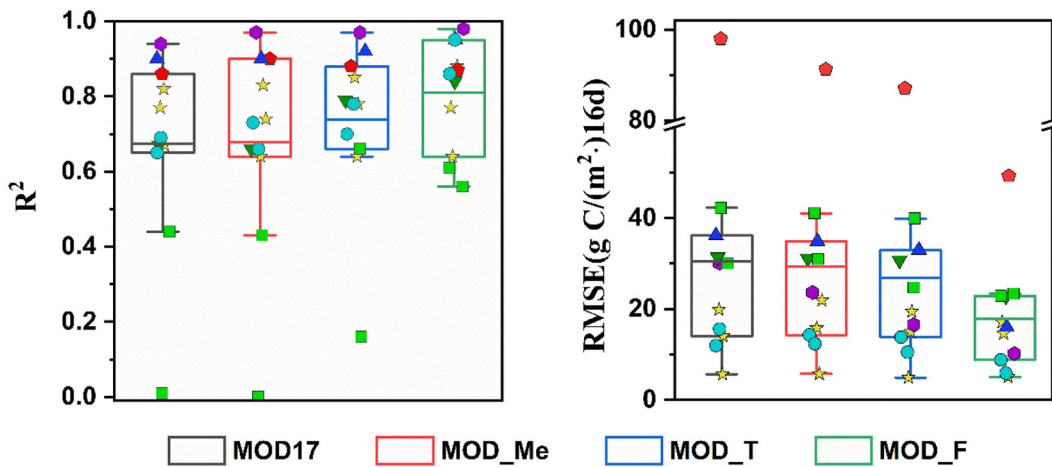
Fig. 5. Validations of four GPP models. The boxplot shows the R^2, and RMSE between 16-day observed GPP and the model estimated GPP for flux-tower sites. The MOD17 is the MODIS GPP model, and MOD_Me is the MODIS GPP model driven by situ meteorological data. The MOD_T and MOD_F are the improved GPP model. The different color symbols in the box indicate the flux sites of different vegetation types, as shown in Fig. 1.
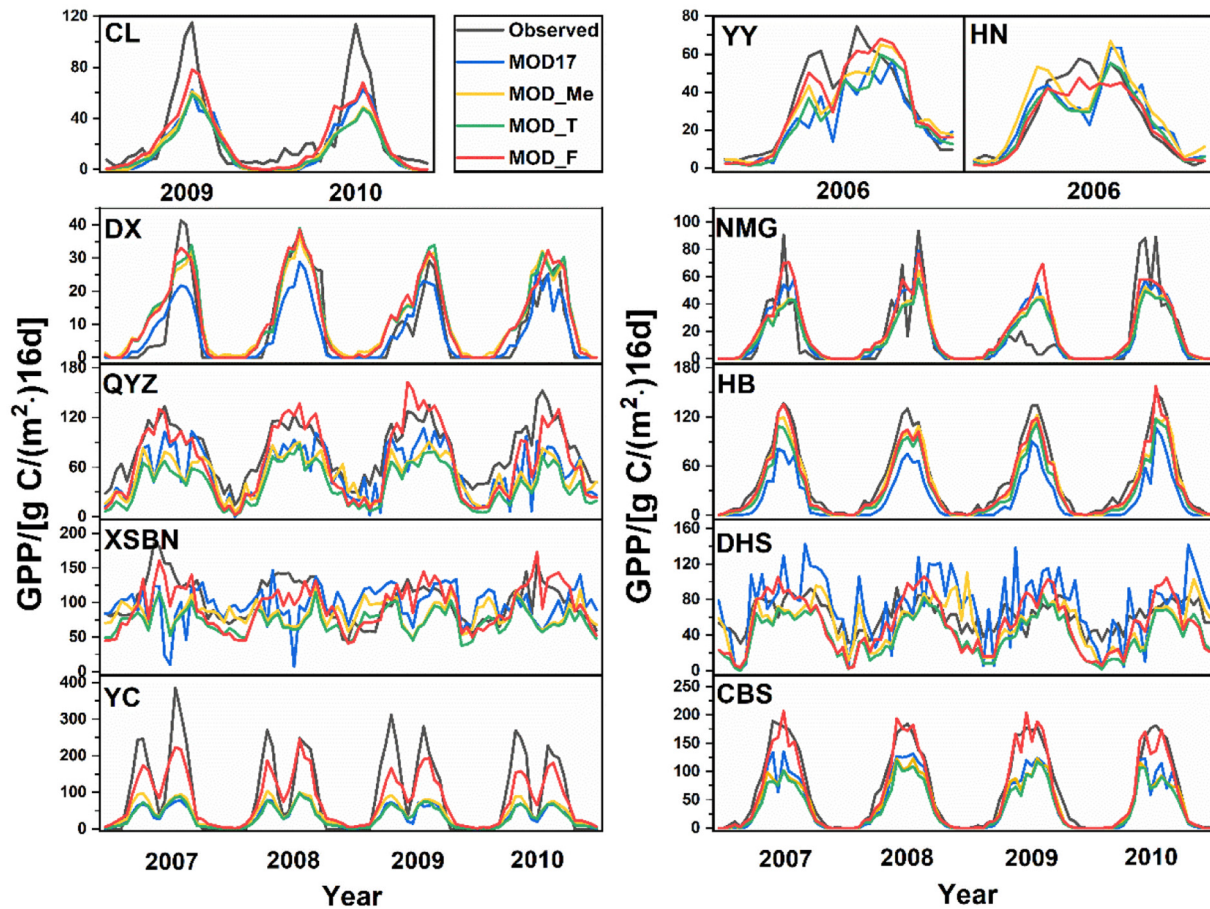
Fig. 6. Comparisons of seasonal variations of observed GPP versus estimated GPP MOD17, MOD_Me, MOD_T and MOD_F at 11 flux tower sites in the validation years (The MOD17 was the MODIS GPP model and MOD_Me was MODIS GPP model driven by in situ meteorological data. The MOD_T and MOD_F are the improved GPP model). DHS, DX, NMG, CL, DL, HB, YC, QYZ, YY, HN, CBS, and XSBN are the flux-tower site ID, and detailed information can be found in Table 1.

the larger increase in GPP is mainly in central China. According to estimates by MOD_F and MOD17, the average annual total GPP over China is 5.7 ± 0.27 and 5 ± 0.24 PgC during 2001–2018, respectively. The GPP estimated by MOD_F in China significantly increases for the 18-year period by 0.046 ± 0.006 PgC year^{-1} (Fig. 7e). The MOD17 also significantly increased during 2001–2018 (0.04 ± 0.006 PgC year^{-1}, $P < 0.001$).

4. Discussion

An understanding of the photosynthesis-temperature relationship is important for improving the estimation of terrestrial ecosystem gross primary productivity. Our results on T_{opt}^{eco} are similar to those of a recent study (Huang et al., 2019), suggesting that the global terrestrial average value of T_{opt}^{eco} is estimated to be 23 ± 6 °C. Evergreen broad-leaved forest also has the largest T_{opt}^{eco}, with a value of 29 ± 3 °C, and the smallest T_{opt}^{eco} (13 ± 3 °C) is in cold grasslands on the Tibetan Plateau. The study by Huang et al. (2019) defines the concept of T_{opt}^{eco} and provides the first global distribution of T_{opt}^{eco}. However, they did not further study the ecosystem-scale minimum and maximum temperature for photosynthesis. We specifically define T_{min}^{eco} and T_{max}^{eco} as "the minimum and maximum air temperature at which gross primary productivity is close to zero within a few years." However, it is harder to detect T_{min}^{eco} than T_{opt}^{eco}. It was found that a robust estimate of T_{opt}^{eco} can be derived at all 11 sites, while there were only four sites for T_{min}^{eco}. T_{min}^{eco} was not detected

in any of the tropical and subtropical sites or most regions. This finding may be related to the influence of the background climate. Generally, when the temperature drops in autumn and winter, especially in the temperate regions of northern China, most of the deciduous plants and trees begin to shed leaves and enter a dormant state to stop growing. The tropical regions have high temperatures throughout the year, with an average annual temperature above 18 °C (Kottek et al., 2006). For example, the average annual temperature at XSBN flux-tower station in the tropical region is about 20 °C, EVI is generally higher than 0.3, and GPP is generally higher than 3 gC m^{-2} d^{-1}. Generally, it is suitable for vegetation growth throughout the year, and vegetation is rarely affected by low-temperature stress; therefore, T_{min}^{eco} cannot be detected. This minimal detection suggests that if T_{min}^{eco} does not reach a lower temperature or experience a long period of low temperature but without impacts on vegetation growth, it will not be detected. In general, the specific definition of T_{min}^{eco} will help promote the study of T_{min}^{eco}, which means that the large-scale spatiotemporal characterization of T_{min}^{eco} can be quantitatively investigated.

T_{max}^{eco} was similar to T_{min}^{eco}; however, it was more challenging to detect than T_{min}^{eco}. T_{max}^{eco} was not detected at all sites and in most areas of China. The main reason may be that it still does not reach the continuous high temperature that will cause vegetation to wither in the study period. This may also be due to the relatively large spatiotemporal scale (16-day, 250 m) of satellite observations, resulting in the information not being captured in time. Additionally, some studies show that it is

Fig. 7. Comparisons of mean annual GPP (a, b), annual GPP temporal trend (c, d) and interannual variations in anomalies of annual total GPP (e) with the improved model (MOD_F) (a, c) and MODIS GPP model (MOD17) (b, d) in China during the period 2001–2018. The inset in panel (a, b) and (c, d) denotes the frequency distribution of the average and temporal trend for annual GPP, respectively. The white-colored areas on land are non-vegetated pixels (a, b). Only grid cells with a significant trend determined by the MK test ($P < 0.05$) are shown in (c, d).
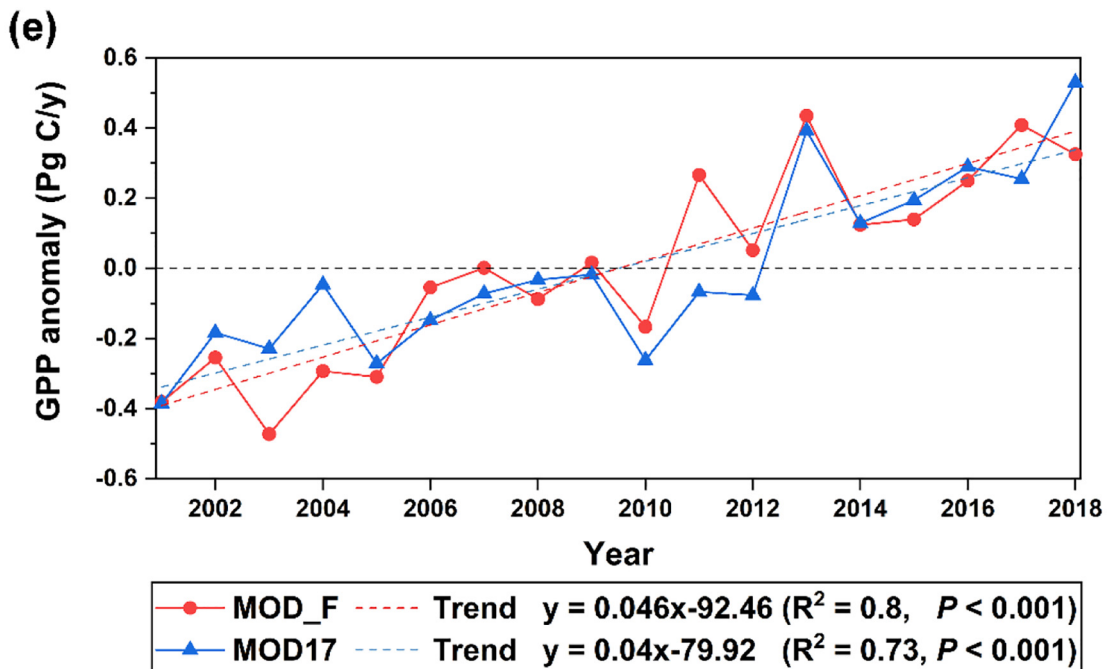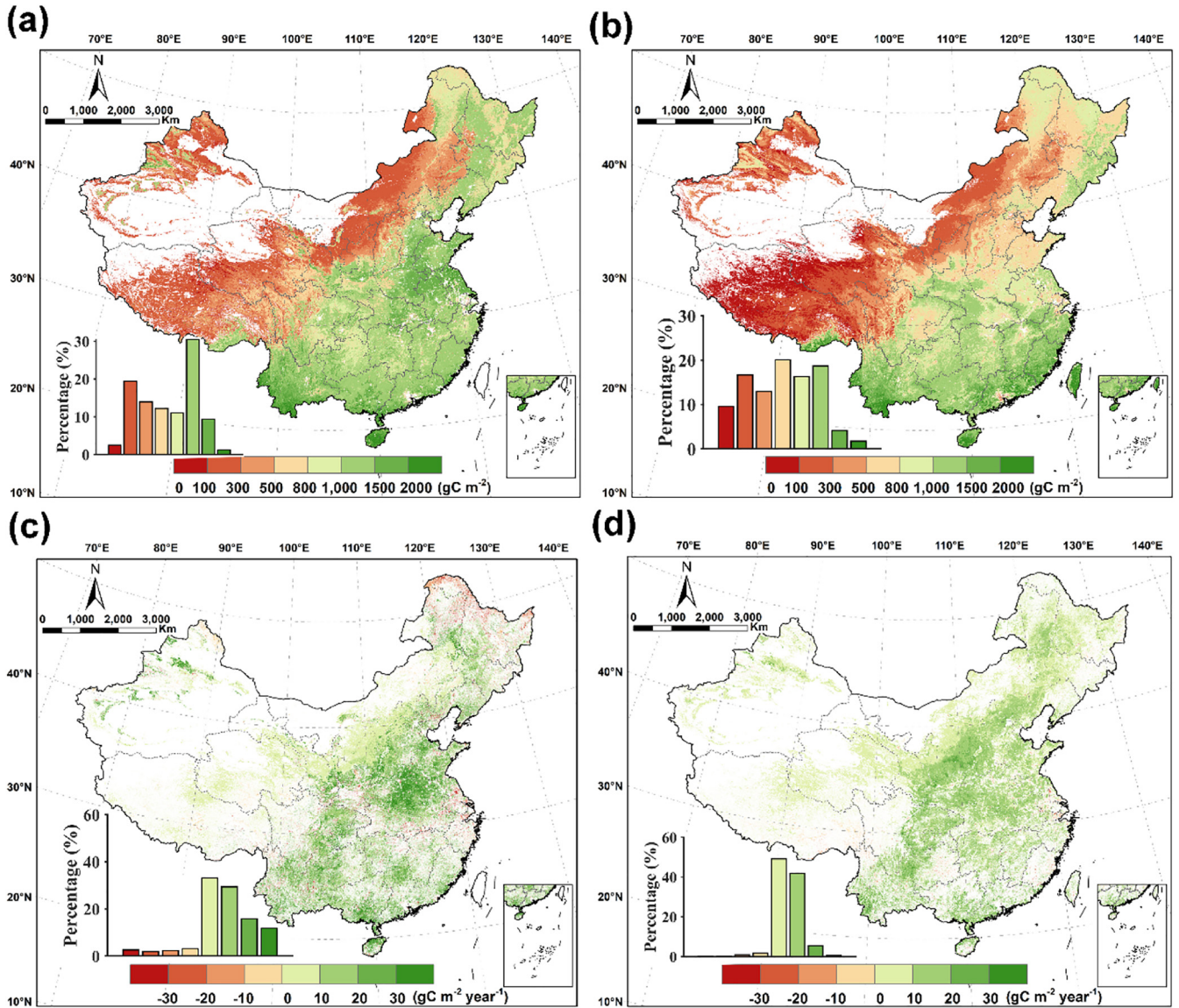
difficult to capture the responses of GPP to short-term high temperatures by modeling methods in a realistic way (Otkin et al., 2018; Zhang et al., 2016). Future climate scenarios unanimously predict global warming, and extreme high-temperature events will gradually intensify (Wu et al., 2019). Thus, it is necessary to use more refined spatiotemporal scale satellite observations and find better methods to detect T_{max}^{eco} in future research. To restore the true relationship between vegetation and temperature in areas where T_{opt}^{eco} and T_{min}^{eco} were not detected, the mean values of T_{opt}^{eco} and T_{min}^{eco} in the regions with the same vegetation type were replaced by NODATA. Here, we assumed that the adaptability of vegetation to temperature conditions was similar within the same vegetation type. Of course, this may also cause a difference in the T_{opt}^{eco} and T_{min}^{eco} due to different climate, latitude, and geographical space (Cui, 2013). Further studies are necessary to gain insights regarding particular eco-geographic regions and obtain more refined eco-geographic regions consistent with a specific climate and ecosystem. Clarifying how terrestrial ecosystem gross primary productivity varies with air temperature is important for understanding and projecting carbon cycle-climate feedbacks.

In addition to the MODIS GPP model, numerous GPP models consider temperature stress, such as the TEC, VPM, EC-LUE, CI-LUE, TL-LUE, and TEM GPP models (He et al., 2013; Raich et al., 1991; Wang et al., 2015; Xiao et al., 2004a; Yan et al., 2015; Yuan et al., 2007). However, these models generally incorporate the photosynthesis-temperature response functions to use the knowledge from the leaf-scale (not ecosystem-scale) to project the GPP response to air temperature at the ecosystem scale (Rogers et al., 2017). These models also usually adopt the constant temperature parameters related to vegetation types to calculate the temperature scalars, without considering the spatial heterogeneity of temperature parameters. Therefore, we studied the ecosystem-scale photosynthesis-temperature response functions and estimated the distribution of T_{opt}^{eco} and T_{min}^{eco} in China. Our improved model was prior to these models in defining the temperature stress factor as $f(T)$ incorporates the photosynthesis-temperature relationship at ecosystem scale. Fig. 4 shows that this improvement had a great performance in expressing the temperature stress effect. The high R^2 and low RMSE between the observed GPP and the improved model estimated GPP (MOD_T) in the flux-tower sites demonstrated the effectiveness of the improved model in GPP estimation (Fig. 5). Most importantly, the original MOD17 neglects the influence of maximum temperature on vegetation photosynthesis and the spatial heterogeneity of these temperature parameters. The improved model considers these and enhances the relevant physiological and ecological mechanisms.

The further addition of FPAR and corresponding LUE$_{max}$ improvements in the MOD_F model produces the best overall statistics for all data (Fig. 5). Moreover, EVI showed a more significant correlation with observed GPP than FPAR (Figs. 4b, S2), especially forest sites. FPAR showed no significant correlations with GPP in evergreen broad-leaf forests (DHS, XSBN); this may cause MOD17 to estimate the GPP of evergreen broad-leaved forests the worst. The MODIS FPAR product algorithm employs a 3D canopy radiative transfer model (Knyazikhin et al., 1998) and a back-up algorithm that uses empirical relationships between the leaf area index (LAI), FPAR, and normalized difference vegetation index (NDVI). One factor may be the saturation of NDVI over dense vegetation and large sensitivity to canopy background brightness (Qi et al., 2019), leading to underestimation of FPAR. However, EVI uses the surface bidirectional reflectance of red and near-infrared spectral bands that are sensitive to leaf chlorophyll content and employs blue spectral reflectance to reduce the impact of atmospheric conditions (Huete et al., 2002). This process improves EVI performance over dense vegetation, makes EVI more sensitive to changes in the crown structure, and provides a reasonably accurate estimation of GPP (Ma et al., 2014; Shi et al., 2017). FPAR has a good correlation with GPP for grassland, shrubland, and farmland, but the model using FPAR still underestimated GPP (Fig. 6). This underestimation may be caused by

the uncertainty of LUE$_{max}$, which is also mentioned in other studies (Marshall et al., 2018; Wang et al., 2015; Yuan et al., 2007). Based on the flux-tower data and genetic algorithm, the LUE$_{max}$ parameters of various vegetation types are re-optimized, and the simulated GPP (MOD_F) then showed good capabilities. In follow-up research, it is still necessary to explore new logic that considers both geospatial and seasonal variations in LUE$_{max}$ parameters.

In short, the two innovations independently played a positive effect in improving GPP estimation. Compared with MOD17, the product from this study (MOD_F) has higher estimates of average annual total GPP over China during 2001–2018, approximately 5.7 ± 0.27 PgC. The results show that Chinese vegetation has great carbon sequestration potential and plays an important role in the global carbon cycle. Although the distribution of the interannual trend of GPP is heterogeneous among different regions from 2001 to 2018, it shows a significant increasing trend at the national scale (Fig. 7). Such results are consistent with previous studies using different GPP models (Li et al., 2013; Ma et al., 2019). Overall, the improved GPP model (MOD_F) provides a reliable GPP estimation for China's terrestrial vegetation and global carbon cycle research.

CRediT authorship contribution statement

Dong Yang: Investigation and performed experiment, Methodology, Data curation, Validation, Writing-original draft. **Xianli Xu:** Conceptualization, Supervised the research and designed experiments, Writing-Reviewing. **Fengjing Xiao**: Conceptualization and Data curation. **Chaohao Xu:** Writing- Reviewing and Editing. **Wei Luo:** Writing-Reviewing and Editing. **Lizhi Tao:** Writing- Reviewing and Editing.

Declaration of competing interest

The authors declare that they have no known competing financial interests or personal relationships that could have appeared to influence the work reported in this paper.

Acknowledgements

Appendix A. Supplementary data

Supplementary data to this article can be found online at https://doi.org/10.1016/j.scitotenv.2021.147805.

References

Aber, J.D., Reich, P.B., Goulden, M.L., 1996. Extrapolating leaf CO₂ exchange to the canopy: a generalized model of forest photosynthesis compared with measurements by eddy correlation. Oecologia 106, 257–265. https://doi.org/10.1007/BF00328606.

Beer, C., Reichstein, M., Tomelleri, E., Ciais, P., Jung, M., Carvalhais, N., et al., 2010. Terrestrial gross carbon dioxide uptake: global distribution and covariation with climate. Science 329, 834–838. https://doi.org/10.1126/science.1184984.

Bjorkman, O., Demmig, B., 1987. Photon yield of O-2 evolution and chlorophyll fluorescence characteristics at 77-K among vascular plants of diverse origins. Planta 170, 489–504. https://doi.org/10.1007/Bf00402983.

Chang, Q., Xiao, X., Wu, X., Doughty, R., Jiao, W., Bajgain, R., et al., 2020. Estimating site-specific optimum air temperature and assessing its effect on the photosynthesis of grasslands in mid- to high-latitudes. Environ. Res. Lett. 15 (3). https://doi.org/10.1088/1748-9326/ab70bb.

Chang, Q., Xiao, X., Doughty, R., Wu, X., Jiao, W., Qin, Y., 2021. Assessing variability of optimum air temperature for photosynthesis across site-years, sites and biomes and their effects on photosynthesis estimation. Agric. For. Meteorol., 298–299 https://doi.org/10.1016/j.agrformet.2020.108277.

Chiang, F., Mazdiyasni, O., AghaKouchak, A., 2018. Amplified warming of droughts in southern United States in observations and model simulations. Sci. Adv. 4. https://doi.org/10.1126/sciadv.aat2380 eaat2380.

Cui, Y., 2013. Preliminary estimation of the realistic optimum temperature for vegetation growth in China. Environ. Manag. 52, 151–162. https://doi.org/10.1007/s00267-013-0065-1.

Didan, K., 2015. In: NELP, D.A.A.C. (Ed.), MOD13Q1 MODIS/Terra Vegetation Indices 16-day L3 Global 250m SIN Grid V006. NASA EOSDIS Land Processes DAAC, NASA EOSDIS Land Processes DAAC.

Fernández-Martínez, M., Vicca, S., Janssens, I.A., Sardans, J., Luyssaert, S., Campioli, M., et al., 2014. Nutrient availability as the key regulator of global forest carbon balance. Nat. Clim. Chang. 4, 471–476. https://doi.org/10.1038/nclimate2177.

Friedl, M., Sulla-Menashe, D., 2019. MCD12Q1 MODIS/Terra+Aqua Land Cover Type Yearly L3 Global 500m SIN Grid V006.

Gao, Y.N., Yu, G.R., Yan, H.M., Zhu, X.J., Li, S.G., Wang, Q.F., et al., 2014. A MODIS-based photosynthetic capacity model to estimate gross primary production in Northern China and the Tibetan Plateau. Remote Sens. Environ. 148, 108–118. https://doi.org/10.1016/j.rse.2014.03.006.

Gitelson, A.A., Vina, A., Verma, S.B., Rundquist, D.C., Arkebauer, T.J., Keydan, G., et al., 2006. Relationship between gross primary production and chlorophyll content in crops: implications for the synoptic monitoring of vegetation productivity. J. Geophys. Res.-Atmos. 111. https://doi.org/10.1029/2005jd006017.

He, M.Z., Ju, W.M., Zhou, Y.L., Chen, J.M., He, H.L., Wang, S.Q., et al., 2013. Development of a two-leaf light use efficiency model for improving the calculation of terrestrial gross primary productivity. Agric. For. Meteorol. 173, 28–39. https://doi.org/10.1016/j.agrformet.2013.01.003.

Heinsch, F.A., Zhao, M.S., Running, S.W., Kimball, J.S., Nemani, R.R., Davis, K.J., et al., 2006. Evaluation of remote sensing based terrestrial productivity from MODIS using regional tower eddy flux network observations. IEEE Trans. Geosci. Remote Sens. 44, 1908–1925. https://doi.org/10.1109/Tgrs.2005.853936.

Houborg, R., Cescatti, A., Migliavacca, M., Kustas, W.P., 2013. Satellite retrievals of leaf chlorophyll and photosynthetic capacity for improved modeling of GPP. Agric. For. Meteorol. 177, 10–23. https://doi.org/10.1016/j.agrformet.2013.04.006.

Huang, M., Piao, S., Ciais, P., Penuelas, J., Wang, X., Keenan, T.F., et al., 2019. Air temperature optima of vegetation productivity across global biomes. Nat. Ecol. Evol. 3, 772–779. https://doi.org/10.1038/s41559-019-0838-x.

Huete, A., Didan, K., Miura, T., Rodriguez, E.P., Gao, X., Ferreira, L.G., 2002. Overview of the radiometric and biophysical performance of the MODIS vegetation indices. Remote Sens. Environ. 83, 195–213 doi:Pii S0034-4257(02)00096-2.

Hunt, E.R., Kelly, R.D., Smith, W.K., Fahnestock, J.T., Welker, J.M., Reiners, W.A., 2004. Estimation of carbon sequestration by combining remote sensing and net ecosystem exchange data for northern mixed-grass prairie and sagebrush-steppe ecosystems. Environ. Manag. 33, S432–S441. https://doi.org/10.1007/s00267-003-9151-0.

Hutchinson, M.F., Xu, T., 2013. Anusplin Version 4.4 User Guide.

Jarvis A, G.E., Reuter, H.I., Nelson, A.D., 2008. Hole-filled SRTM for the Globe: Version 4.

Jonsson, P., Eklundh, L., 2004. TIMESAT - a program for analyzing time-series of satellite sensor data. Comput. Geosci. 30, 833–845. https://doi.org/10.1016/j.cageo.2004.05.006.

Kattge, J., Knorr, W., 2007. Temperature acclimation in a biochemical model of photosynthesis: a reanalysis of data from 36 species. Plant Cell Environ. 30, 1176–1190. https://doi.org/10.1111/j.1365-3040.2007.01690.x.

Kattge, J., Knorr, W., Raddatz, T., Wirth, C., 2009. Quantifying photosynthetic capacity and its relationship to leaf nitrogen content for global-scale terrestrial biosphere models. Glob. Chang. Biol. 15, 976–991. https://doi.org/10.1111/j.1365-2486.2008.01744.x.

Kendall, M.G., 1975. Rank Correlation Methods. 4th edition. Charles Griffin, London.

Knyazikhin, Y., Martonchik, J.V., Myneni, R.B., Diner, D.J., Running, S.W., 1998. Synergistic algorithm for estimating vegetation canopy leaf area index and fraction of absorbed photosynthetically active radiation from MODIS and MISR data. J. Geophys. Res.-Atmos. 103, 32257–32275. https://doi.org/10.1029/98jd02462.

Kottek, M., Grieser, J., Beck, C., Rudolf, B., Rubel, F., 2006. World map of the Köppen-Geiger climate classification updated. Meteorol. Z. 15, 259–263. https://doi.org/10.1127/0941-2948/2006/0130.

Li, X., Xiao, J., 2019. A global, 0.05-degree product of solar-induced chlorophyll fluorescence derived from OCO-2, MODIS, and reanalysis data. Remote Sens. 11. https://doi.org/10.3390/rs11050517.

Li, X., Liang, S., Yu, G., 2013. Estimations of gross primary production over the terrestrial ecosystems in China. Ecol. Model. 261-262 (1), 80–92. https://doi.org/10.1016/j.ecolmodel.2013.03.024.

Liu, Y.W., 2020. Optimum temperature for photosynthesis: from leaf- to ecosystem-scale. Sci. Bull. 65, 601–604. https://doi.org/10.1016/j.scib.2020.01.006.

Liu, Y.W., Piao, S.L., Lian, X., Ciais, P., Smith, W.K., 2017. Seasonal responses of terrestrial carbon cycle to climate variations in CMIP5 models: evaluation and projection. J. Clim. 30, 6481–6503. https://doi.org/10.1175/Jcli-D-16-0555.1.

Liu, Z.J., Wang, L.C., Wang, S.S., 2014. Comparison of different GPP models in China using MODIS image and ChinaFLUX data. Remote Sens. 6, 10215–10231. https://doi.org/10.3390/rs61010215.

Ma, J., Xiao, X., Miao, R., Li, Y., Chen, B., Zhang, Y., et al., 2019. Trends and controls of terrestrial gross primary productivity of China during 2000–2016. Environ. Res. Lett. 14. https://doi.org/10.1088/1748-9326/ab31e4.

Ma, X., Huete, A., Yu, Q., Restrepo-Coupe, N., Beringer, J., Hutley, L.B., et al., 2014. Parameterization of an ecosystem light-use-efficiency model for predicting savanna GPP using MODIS EVI. Remote Sens. Environ. 154, 253–271. https://doi.org/10.1016/j.rse.2014.08.025.

Mann, H.B., 1945. Nonparametric tests against trend. Econometrica 13, 245–259. https://doi.org/10.2307/1907187.

Marshall, M., Tu, K., Brown, J., 2018. Optimizing a remote sensing production efficiency model for macro-scale GPP and yield estimation in agroecosystems. Remote Sens. Environ. 217, 258–271. https://doi.org/10.1016/j.rse.2018.08.001.

McGuire, A.D., Melillo, J.M., Joyce, L.A., Kicklighter, D.W., Grace, A.L., Moore, B., et al., 1992. Interactions between carbon and nitrogen dynamics in estimating net primary productivity for potential vegetation in North America. Glob. Biogeochem. Cycles 6, 101–124. https://doi.org/10.1029/92gb00219.

Monteith, J.L., 1972. Solar-radiation and productivity in tropical ecosystems. J. Appl. Ecol. 9, 747–766. https://doi.org/10.2307/2401901.

Moriasi, D.N., Arnold, J.G., Van Liew, M.W., Bingner, R.L., Harmel, R.D., Veith, T.L., 2007. Model evaluation guidelines for systematic quantification of accuracy in watershed simulations. Trans. ASABE 50, 885–900. https://doi.org/10.13031/2013.23153.

Myneni, R., Knyazikhin, Y., Park, T., 2015. In: NELP, D.A.A.C. (Ed.), MOD15A2H MODIS/Terra Leaf Area Index/FPAR 8-day L4 Global 500m SIN Grid V006. NASA EOSDIS Land Processes DAAC, NASA EOSDIS Land Processes DAAC.

Niu, S., Luo, Y., Fei, S., Yuan, W., Schimel, D., Law, B.E., et al., 2012. Thermal optimality of net ecosystem exchange of carbon dioxide and underlying mechanisms. New Phytol. 194, 775–783. https://doi.org/10.1111/j.1469-8137.2012.04095.x.

Ogutu, B.O., Dash, J., 2013. Assessing the capacity of three production efficiency models in simulating gross carbon uptake across multiple biomes in conterminous USA. Agric. For. Meteorol. 174, 158–169. https://doi.org/10.1016/j.agrformet.2013.02.016.

Ogutu, B.O., Dash, J., Dawson, T.P., 2013. Developing a diagnostic model for estimating terrestrial vegetation gross primary productivity using the photosynthetic quantum yield and Earth Observation data. Glob. Chang. Biol. 19, 2878–2892. https://doi.org/10.1111/gcb.12261.

Otkin, J.A., Svoboda, M., Hunt, E.D., Ford, T.W., Anderson, M.C., Hain, C., et al., 2018. Flash droughts: a review and assessment of the challenges imposed by rapid-onset droughts in the United States. Bull. Am. Meteorol. Soc. 99, 911–919. https://doi.org/10.1175/bams-d-17-0149.1.

Papale, D., Reichstein, M., Aubinet, M., Canfora, E., Bernhofer, C., Kutsch, W., et al., 2006. Towards a standardized processing of Net Ecosystem Exchange measured with eddy covariance technique: algorithms and uncertainty estimation. Biogeosciences 3, 571–583. https://doi.org/10.5194/bg-3-571-2006.

Pastorello, G., Trotta, C., Canfora, E., et al., 2020. The FLUXNET2015 dataset and the ONEFlux processing pipeline for eddy covariance data. Sci. Data 7, 225. https://doi.org/10.1038/s41597-020-0534-3.

Piao, S., Fang, J., Ciais, P., Peylin, P., Huang, Y., Sitch, S., et al., 2009. The carbon balance of terrestrial ecosystems in China. Nature 458, 1009–1013. https://doi.org/10.1038/nature07944.

Pohlheim, H., 2006. GEATbx: Genetic and Evolutionary Algorithm Toolbox for Use With Matlab. https://doi.org/10.1007/978-3-642-57137-4_6.

Potter, C.S., Randerson, J.T., Field, C.B., Matson, P.A., Vitousek, P.M., Mooney, H.A., et al., 1993. Terrestrial ecosystem production - a process model-based on global satellite and surface data. Glob. Biogeochem. Cycles 7, 811–841. https://doi.org/10.1029/93gb02725.

Qi, X., Jia, J., Liu, H., Lin, Z., 2019. Relative importance of climate change and human activities for vegetation changes on China's silk road economic belt over multiple timescales. Catena.180, 224–237. https://doi.org/10.1016/j.catena.2019.04.027.

Raich, J.W., Rastetter, E.B., Melillo, J.M., Kicklighter, D.W., Steudler, P.A., Peterson, B.J., et al., 1991. Potential net primary productivity in South America: application of a global model. Ecol. Appl. 1, 399–429. https://doi.org/10.2307/1941899.

Rogers, A., Medlyn, B.E., Dukes, J.S., Bonan, G., von Caemmerer, S., Dietze, M.C., et al., 2017. A roadmap for improving the representation of photosynthesis in Earth system models. New Phytol. 213, 22–42. https://doi.org/10.1111/nph.14283.

Running, S., Zhao, M., 2019. MOD17A2HGF MODIS/Terra Gross Primary Productivity Gap-filled 8-day L4 Global 500 m SIN Grid V006.

Running, S.W., Thornton, P.E., Nemani, R., JMJMiES, Glassy, 2000. Global terrestrial gross and net primary productivity from the Earth Observing System. Method in Ecosystem Science, pp. 44–57 https://doi.org/10.1007/978-1-4612-1224-9_4.

Running, S.W., Nemani, R.R., Heinsch, F.A., Zhao, M.S., Reeves, M., Hashimoto, H., 2004. A continuous satellite-derived measure of global terrestrial primary production. Bioscience 54, 547–560. https://doi.org/10.1641/0006-3568(2004)054[0547:Acsmog]2.0.Co;2.

Seddon, A.W., Macias-Fauria, M., Long, P.R., Benz, D., Willis, K.J., 2016. Sensitivity of global terrestrial ecosystems to climate variability. Nature 531, 229–232. https://doi.org/10.1038/nature16986.

Shi, H., Li, L.H., Eamus, D., Huete, A., Cleverly, J., Tian, X., et al., 2017. Assessing the ability of MODIS EVI to estimate terrestrial ecosystem gross primary production of multiple land cover types. Ecol. Indic. 72, 153–164. https://doi.org/10.1016/j.ecolind.2016.08.022.

Sims, D.A., Rahman, A.F., Cordova, V.D., El-Masri, B.Z., Baldocchi, D.D., Flanagan, L.B., et al., 2006. On the use of MODIS EVI to assess gross primary productivity of North American ecosystems. J. Geophys. Res. Biogeosci. 111. https://doi.org/10.1029/2006jg000162.

Sims, D.A., Rahman, A.F., Cordova, V.D., El-Masri, B.Z., Baldocchi, D.D., Bolstad, P.V., et al., 2008. A new model of gross primary productivity for North American ecosystems based solely on the enhanced vegetation index and land surface temperature from MODIS. Remote Sens. Environ. 112, 1633–1646. https://doi.org/10.1016/j.rse.2007.08.004.

Smith, N.G., Malyshev, S.L., Shevliakova, E., Kattge, J., Dukes, J.S., 2016. Foliar temperature acclimation reduces simulated carbon sensitivity to climate. Nat. Clim. Chang. 6, 407–411. https://doi.org/10.1038/Nclimate2878.

Turner, D.P., Ritts, W.D., Cohen, W.B., Gower, S.T., Running, S.W., Zhao, M.S., et al., 2006. Evaluation of MODIS NPP and GPP products across multiple biomes. Remote Sens. Environ. 102, 282–292. https://doi.org/10.1016/j.rse.2006.02.017.

Wang, J., Dong, J., Yi, Y., Lu, G., Oyler, J., Smith, W.K., et al., 2017. Decreasing net primary production due to drought and slight decreases in solar radiation in China from 2000 to 2012. J. Geophys. Res. Biogeosci. 122, 261–278. https://doi.org/10.1002/2016jg003417.

Wang, J., Feng, L., Palmer, P.I., Liu, Y., Fang, S., Bosch, H., et al., 2020. Large Chinese land carbon sink estimated from atmospheric carbon dioxide data. Nature 586, 720–723. https://doi.org/10.1038/s41586-020-2849-9.

Wang, S.Q., Huang, K., Yan, H., Yan, H.M., Zhou, L., Wang, H.M., et al., 2015. Improving the light use efficiency model for simulating terrestrial vegetation gross primary production by the inclusion of diffuse radiation across ecosystems in China. Ecol. Complex. 23, 1–13. https://doi.org/10.1016/j.ecocom.2015.04.004.

White, M.A., Thornton, P.E., Running, S.W., Nemani, R.R., 2000. Parameterization and sensitivity analysis of the BIOME–BGC terrestrial ecosystem model: net primary production controls. Earth Interact. 4, 1–85. https://doi.org/10.1175/1087-3562(2000)004<0003:Pasaot>2.0.Co;2.

Wu, J., Albert, L.P., Lopes, A.P., Restrepo-Coupe, N., Hayek, M., Wiedemann, K.T., et al., 2016. Leaf development and demography explain photosynthetic seasonality in Amazon evergreen forests. Science 351, 972–976. https://doi.org/10.1126/science.aad5068.

Wu, S.H., Yin, Y.H., Zhao, D.S., Huang, M., Shao, X.M., Dai, E.F., 2010. Impact of future climate change on terrestrial ecosystems in China. Int. J. Climatol. 30, 866–873. https://doi.org/10.1002/joc.1938.

Wu, X., Guo, W., Liu, H., Li, X., Peng, C., Allen, C.D., et al., 2019. Exposures to temperature beyond threshold disproportionately reduce vegetation growth in the northern hemisphere. Natl. Sci. Rev. 6, 786–795. https://doi.org/10.1093/nsr/nwy158.

Xiao, X.M., Hollinger, D., Aber, J., Goltz, M., Davidson, E.A., Zhang, Q.Y., et al., 2004a. Satellite-based modeling of gross primary production in an evergreen needleleaf forest. Remote Sens. Environ. 89, 519–534. https://doi.org/10.1016/j.rse.2003.11.008.

Xiao, X.M., Zhang, Q.Y., Braswell, B., Urbanski, S., Boles, S., Wofsy, S., et al., 2004b. Modeling gross primary production of temperate deciduous broadleaf forest using satellite images and climate data. Remote Sens. Environ. 91, 256–270. https://doi.org/10.1016/j.rse.2004.03.010.

Xie, X.M., He, B., Guo, L.L., Miao, C.Y., Zhang, Y.F., 2019. Detecting hotspots of interactions between vegetation greenness and terrestrial water storage using satellite observations. Remote Sens. Environ. 231. https://doi.org/10.1016/j.rse.2019.111259.

Xu, C.H., Xu, X.L., Liu, M.X., Li, Z.W., Zhang, Y.H., Zhu, J.X., et al., 2020. An improved optimization scheme for representing hillslopes and depressions in karst hydrology. Water Resour. Res. 56. https://doi.org/10.1029/2019WR026038.

Yan, H., Wang, S.Q., Billesbach, D., Oechel, W., Bohrer, G., Meyers, T., et al., 2015. Improved global simulations of gross primary product based on a new definition of water stress factor and a separate treatment of C3 and C4 plants. Ecol. Model. 297, 42–59. https://doi.org/10.1016/j.ecolmodel.2014.11.002.

Yao, Y., Li, Z., Wang, T., Chen, A., Wang, X., Du, M., et al., 2018. A new estimation of China's net ecosystem productivity based on eddy covariance measurements and a model tree ensemble approach. Agric. For. Meteorol. 253-254, 84–93. https://doi.org/10.1016/j.agrformet.2018.02.007.

Yu, G.R., Zhu, X.J., Fu, Y.L., He, H.L., Wang, Q.F., Wen, X.F., et al., 2013. Spatial patterns and climate drivers of carbon fluxes in terrestrial ecosystems of China. Glob. Chang. Biol. 19, 798–810. https://doi.org/10.1111/gcb.12079.

Yuan, W., Cai, W., Xia, J., Chen, J., Liu, S., Dong, W., et al., 2014. Global comparison of light use efficiency models for simulating terrestrial vegetation gross primary production based on the LaThuile database. Agric. For. Meteorol. 192-193, 108–120. https://doi.org/10.1016/j.agrformet.2014.03.007.

Yuan, W.P., Liu, S., Zhou, G.S., Zhou, G.Y., Tieszen, L.L., Baldocchi, D., et al., 2007. Deriving a light use efficiency model from eddy covariance flux data for predicting daily gross primary production across biomes. Agric. For. Meteorol. 143, 189–207. https://doi.org/10.1016/j.agrformet.2006.12.001.

Zhang, F.M., Chen, J.M., Chen, J.Q., Gough, C.M., Martin, T.A., Dragoni, D., 2012. Evaluating spatial and temporal patterns of MODIS GPP over the conterminous US against flux measurements and a process model. Remote Sens. Environ. 124, 717–729. https://doi.org/10.1016/j.rse.2012.06.023.

Zhang, Q., Middleton, E.M., Margolis, H.A., Drolet, G.G., Barr, A.A., Black, T.A., 2009. Can a satellite-derived estimate of the fraction of PAR absorbed by chlorophyll (FAPARchl) improve predictions of light-use efficiency and ecosystem photosynthesis for a boreal aspen forest? Remote Sens. Environ. 113, 880–888. https://doi.org/10.1016/j.rse.2009.01.002.

Zhang, Q.Y., Cheng, Y.B., Lyapustin, A.I., Wang, Y.J., Gao, F., Suyker, A., et al., 2014. Estimation of crop gross primary production (GPP): fAPAR(chl) versus MOD15A2 FPAR. Remote Sens. Environ. 153, 1–6. https://doi.org/10.1016/j.rse.2014.07.012.

Zhang, Y., Xiao, X., Zhou, S., Ciais, P., McCarthy, H., Luo, Y., 2016. Canopy and physiological controls of GPP during drought and heat wave. Geophys. Res. Lett. 43, 3325–3333. https://doi.org/10.1002/2016gl068501.

Zhang, Y.Q., Yu, Q., Jiang, J., Tang, Y.H., 2008. Calibration of Terra/MODIS gross primary production over an irrigated cropland on the North China Plain and an alpine meadow on the Tibetan Plateau. Glob. Chang. Biol. 14, 757–767. https://doi.org/10.1111/j.1365-2486.2008.01538.x.

Zhao, M.S., Heinsch, F.A., Nemani, R.R., Running, S.W., 2005. Improvements of the MODIS terrestrial gross and net primary production global data set. Remote Sens. Environ. 95, 164–176. https://doi.org/10.1016/j.rse.2004.12.011.

Zhou, L., Wang, S., Chi, Y., Li, Q., Huang, K., Yu, Q., 2015. Responses of photosynthetic parameters to drought in subtropical forest ecosystem of China. Sci. Rep. 5, 18254. https://doi.org/10.1038/srep18254.

Zhou, S., Zhang, Y., Ciais, P., Xiao, X., Luo, Y., Caylor, K.K., et al., 2017. Dominant role of plant physiology in trend and variability of gross primary productivity in North America. Sci. Rep. 7, 41366. https://doi.org/10.1038/srep41366.